

Supporting Information

Photonic actuators with predefined shapes

Na Yang, Xingxiang Ji, Juanjuan Sun, Yu Zhang, Qinghua Xu, Yingjuan Fu, Hongguang Li,
Menghua Qin, Zaiwu Yuan**

Table of contents

1. Photos of different colloidal suspensions (Fig. S1)
2. N₂ adsorption/desorption measurements of phenol-formaldehyde film with and without GO dried by air or SCCO₂ (Fig. S2, S3)
3. Additional evidences denoting the presence of the N* structure by SEM and CD spectra (Fig. S4-6)
4. Additional proofs from POM and SEM observations denoting the different morphologies of the top and bottom surfaces of the PG film (Fig. S7, S8)
5. Properties of the PGC and PG films (Fig. S9, Fig. S10)
6. Characterizations of the FoA-treated film (Fig. S11-16)
7. Additional results of the tests on the objects treated with different chemicals and those prepared from different films (Fig. S17-23)

1. Photos of different colloidal suspensions

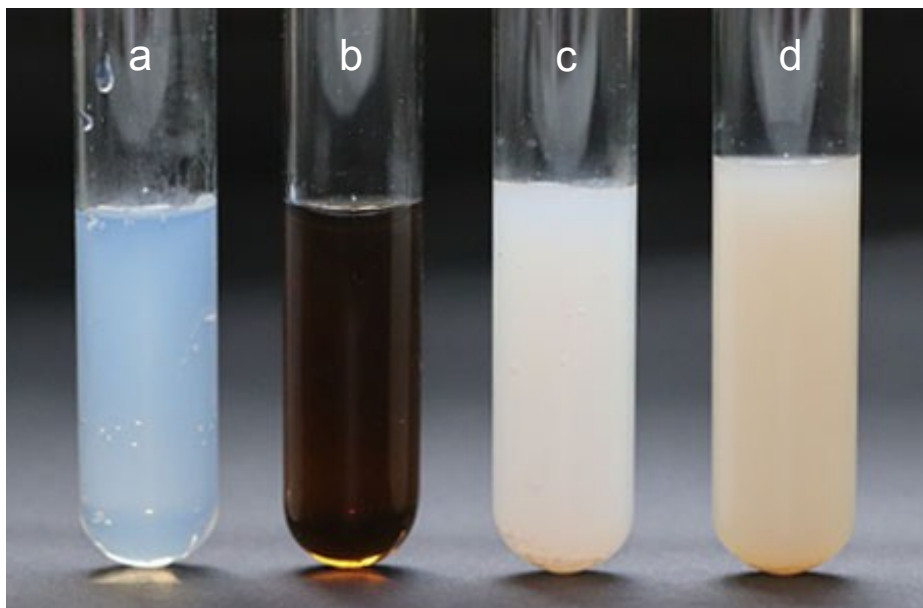


Fig. S1 Photos of a) an aqueous suspension of CNCs (3.5 wt%), b) an aqueous dispersion of GO (0.1 wt%), c) a suspension of *p*-PFR/CNCs by adding 150 μL *p*-PFR in ethanol to 10 mL CNCs suspension and d) a suspension of *p*-PFR/GO/CNCs by further adding 700 μL GO dispersion. Photos were taken immediately after sample preparation by transferring a part of each colloidal suspension into a test tube.

2. N₂ adsorption/desorption measurements of phenol-formaldehyde film with and without GO dried by air or SCCO₂

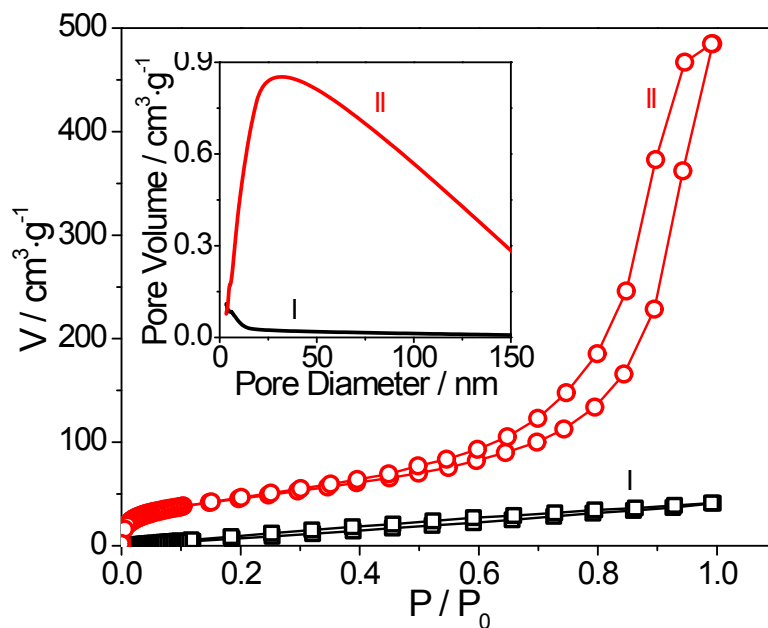


Fig. S2 N₂ adsorption/desorption isotherms of PG3 (curve I) and the film with the same composition but dried by SCCO₂ (curve II). Inset graph denotes corresponding BJH pore size distributions.

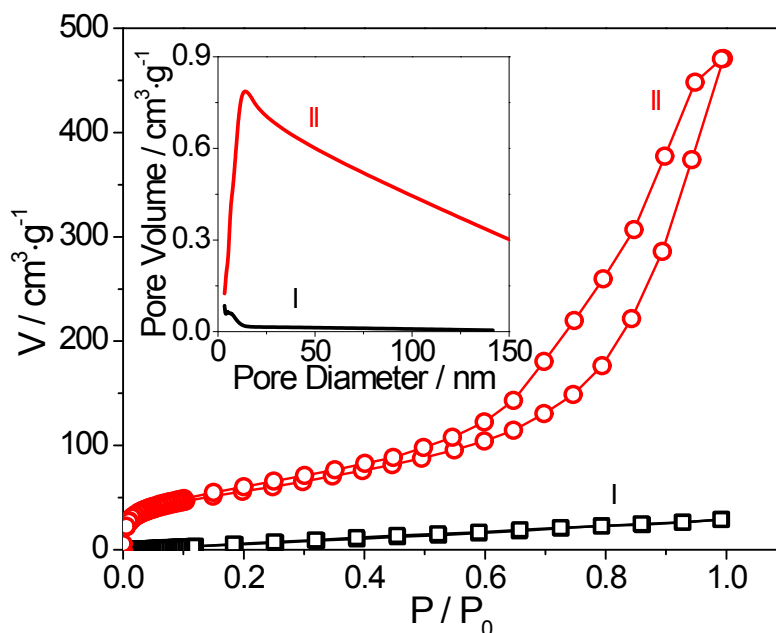


Fig. S3 N₂ adsorption/desorption isotherms of PG0 (curve I) and the film with the same composition but dried by SCCO₂ (curve II). Inset graph denotes corresponding BJH pore size distributions.

3. Additional evidences denoting the presence of the N* structure by SEM and CD spectra

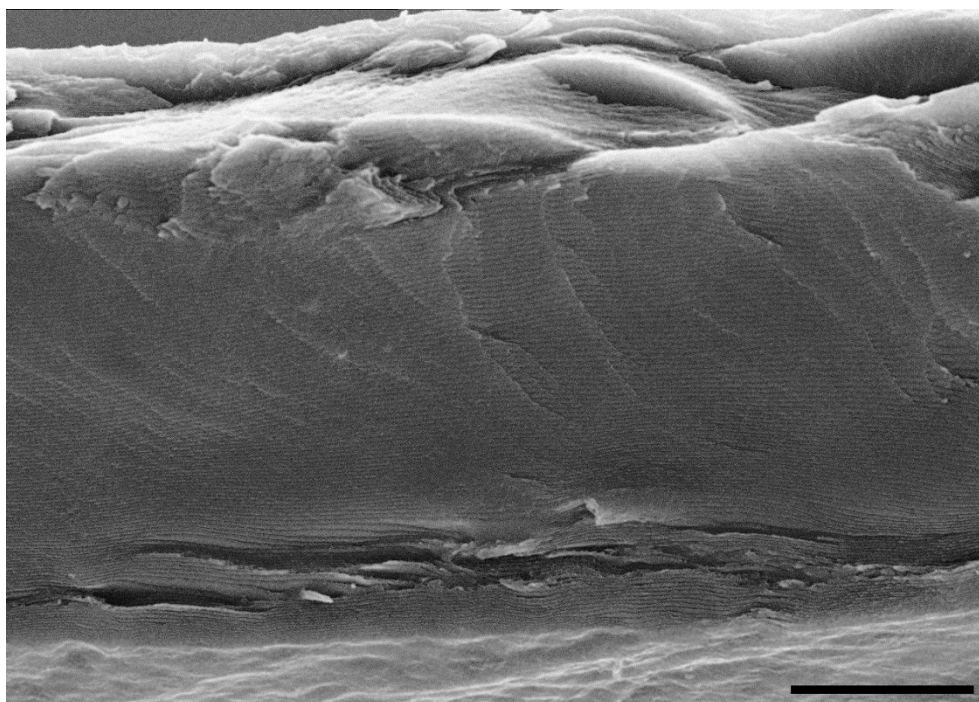


Fig. S4 A typical SEM image of PG0. The scale bar corresponds to 20 μm .

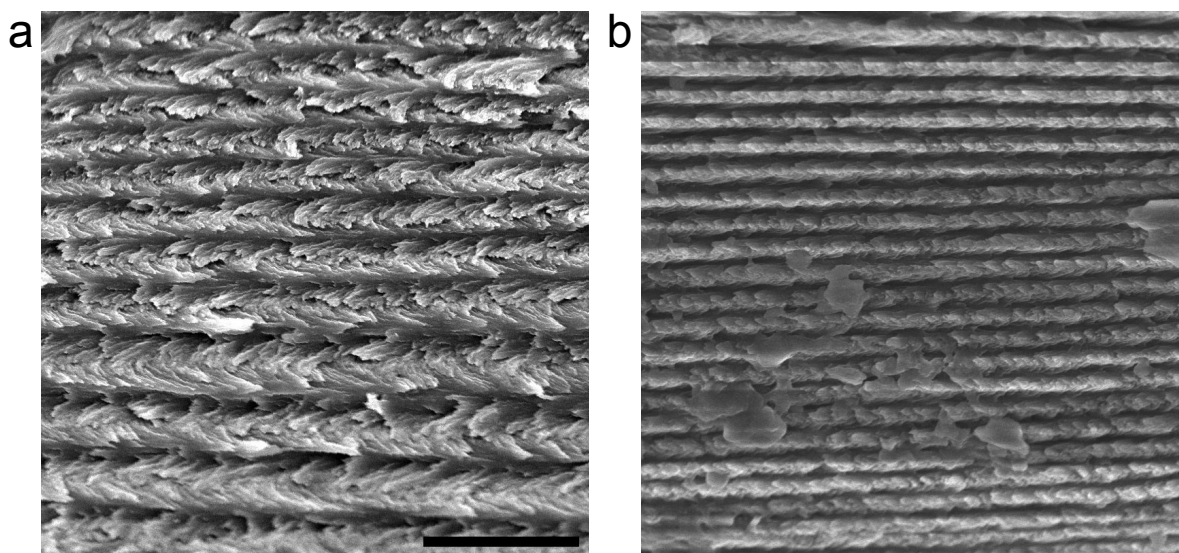


Fig. S5 Typical SEM images of PGC1 (a) and PG1 (b). The magnifications of the two images are the same with the scale bar to be 2.5 μm .

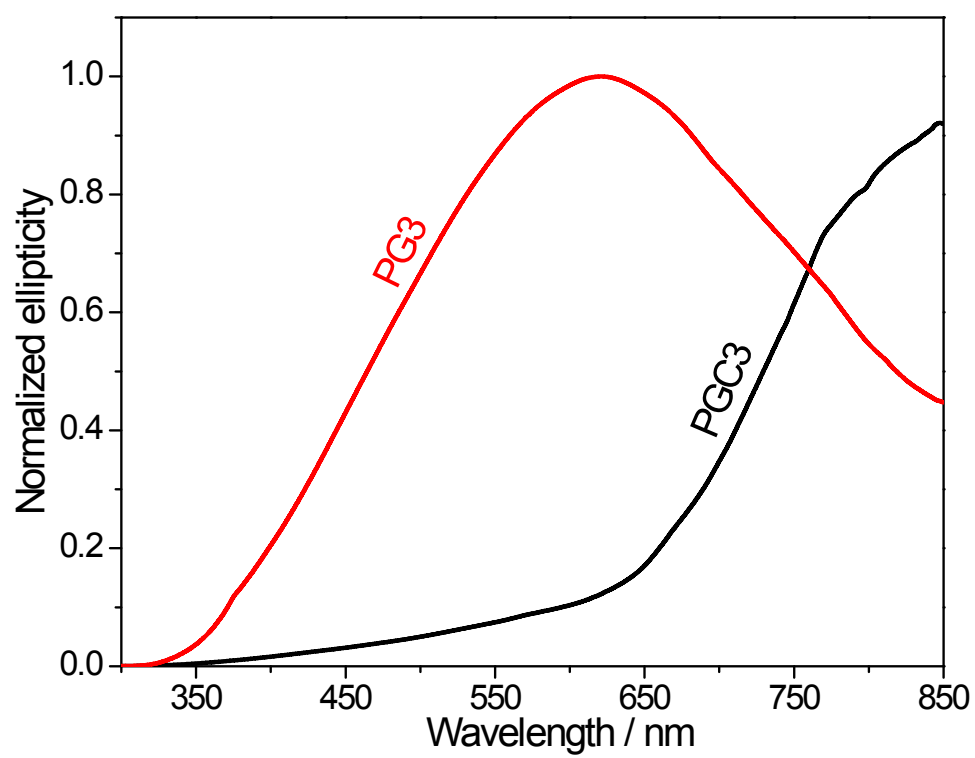


Fig. S6 CD spectra of PGC3 and PG3.

4. Additional proofs from POM and SEM observations denoting the different morphologies of the top and bottom surfaces of the PG film

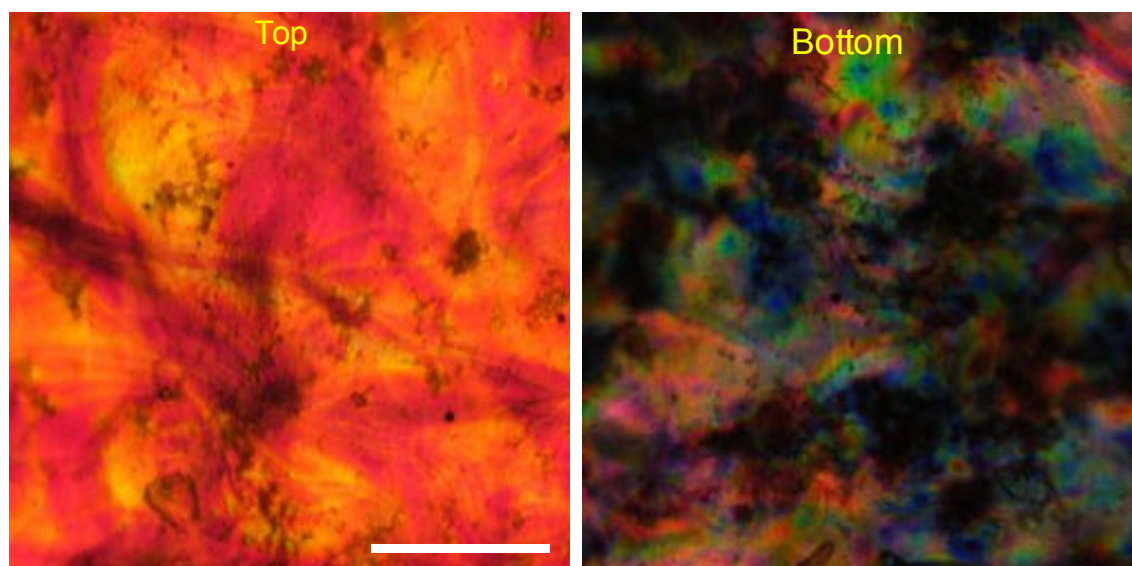


Fig. S7 Polarized microscopy images of the top and bottom surfaces of PG3 as indicated. The magnifications of the two images are the same with the scale bar to be 50 μm .

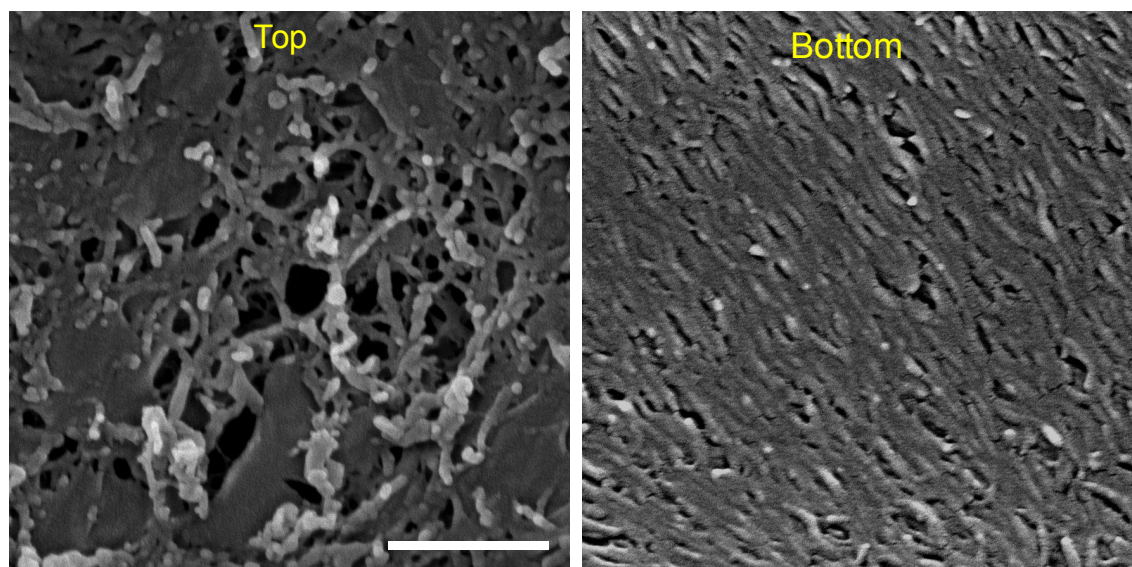


Fig. S8 SEM images of the top and bottom surfaces as indicated of a film with the same composition as that of PG3 but dried by SCCO_2 . The magnifications of the two images are the same with the scale bar to be 500 nm.

5 Properties of the PGC and PG films

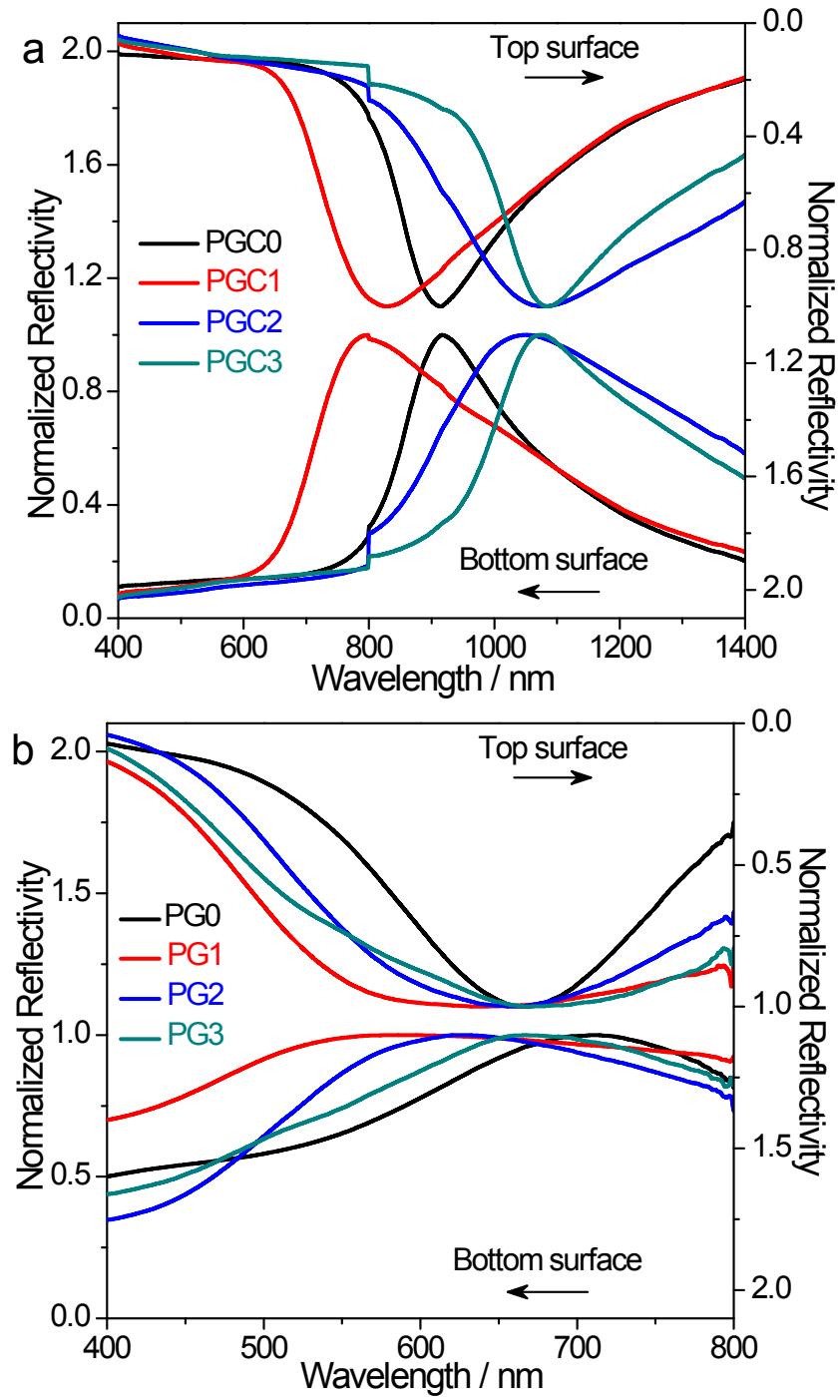


Fig. S9 Normalized reflection spectra of PGC (a) and PG (b) films on both surfaces.

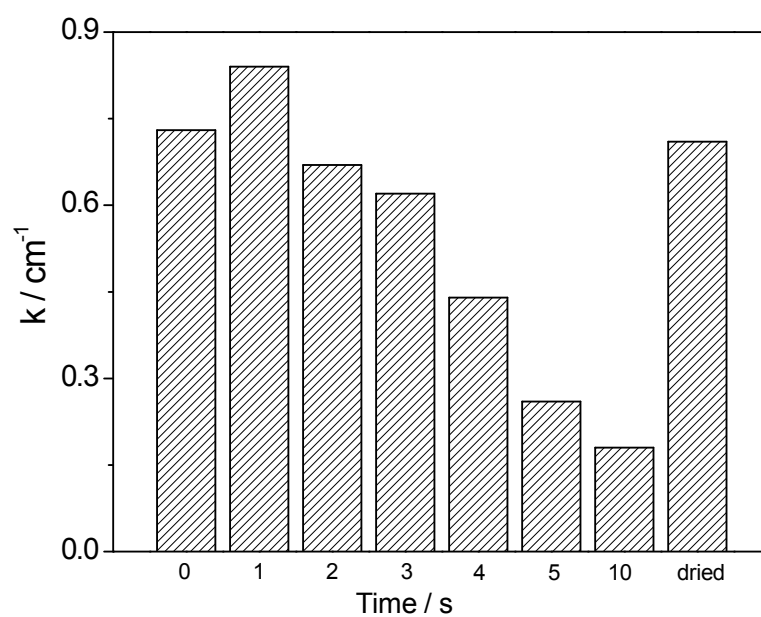


Fig. S10 The change of curvature (κ) with time for the PG3 film bar with a width of 1.5 mm and a thickness of 53 μm immersed in water. The value after total drying is also given for comparison.

6. Characterizations of the FoA-treated film

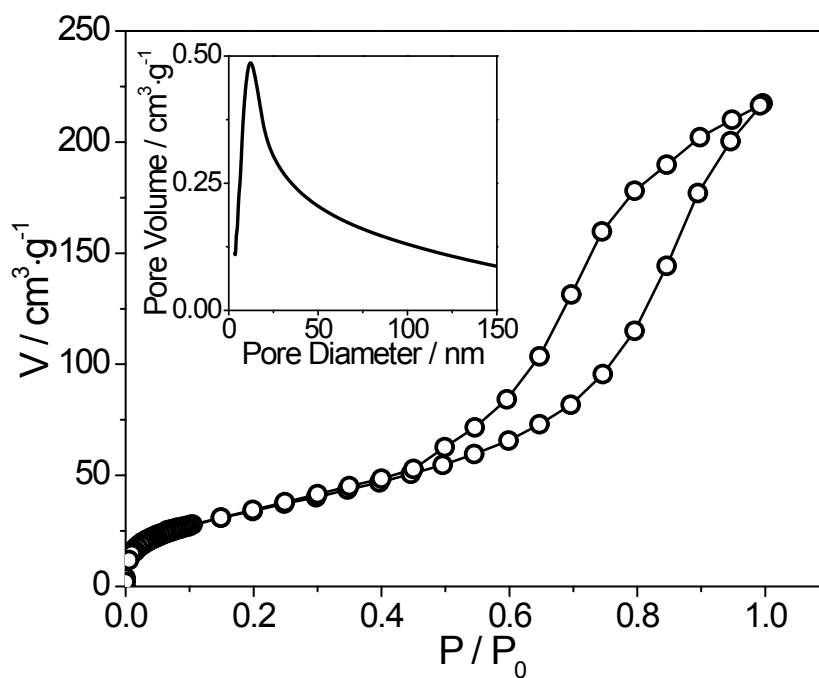


Fig. S11 N₂ adsorption/desorption isotherm and the BJH pore size distribution (inset) of the FoA-soaked film which was dried by SCCO₂. The film has the same composition as that in PG3.

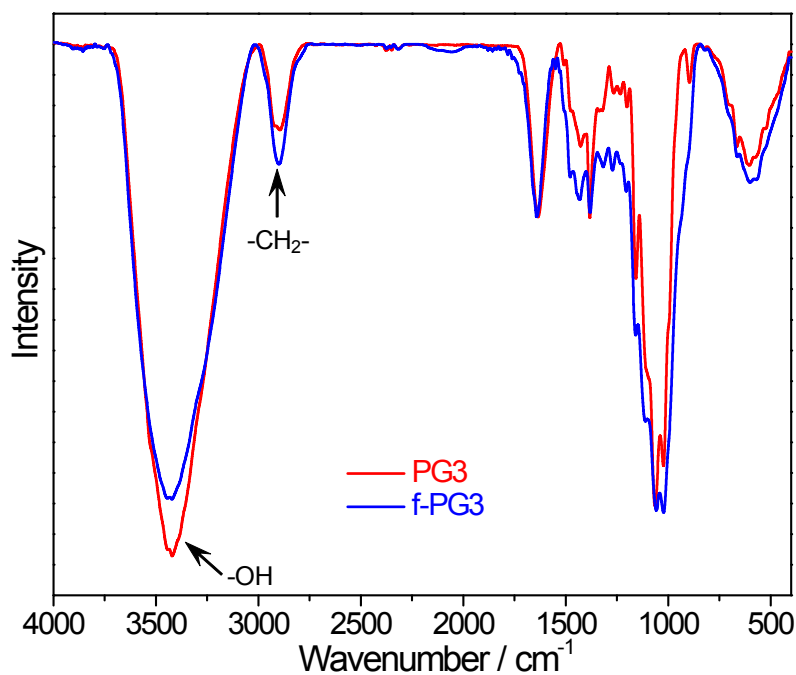


Fig. S12 FTIR spectra of PG3 and f-PG3. The spectra are normalized at 1638 cm^{-1} for better comparison.

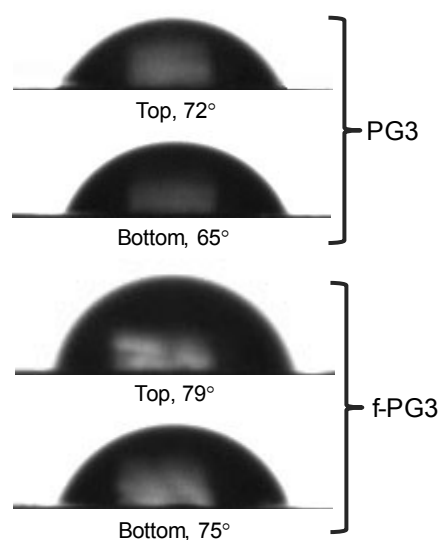


Fig. S13 Water contact angle of PG3 and f-PG3 on top and bottom surfaces as indicated.

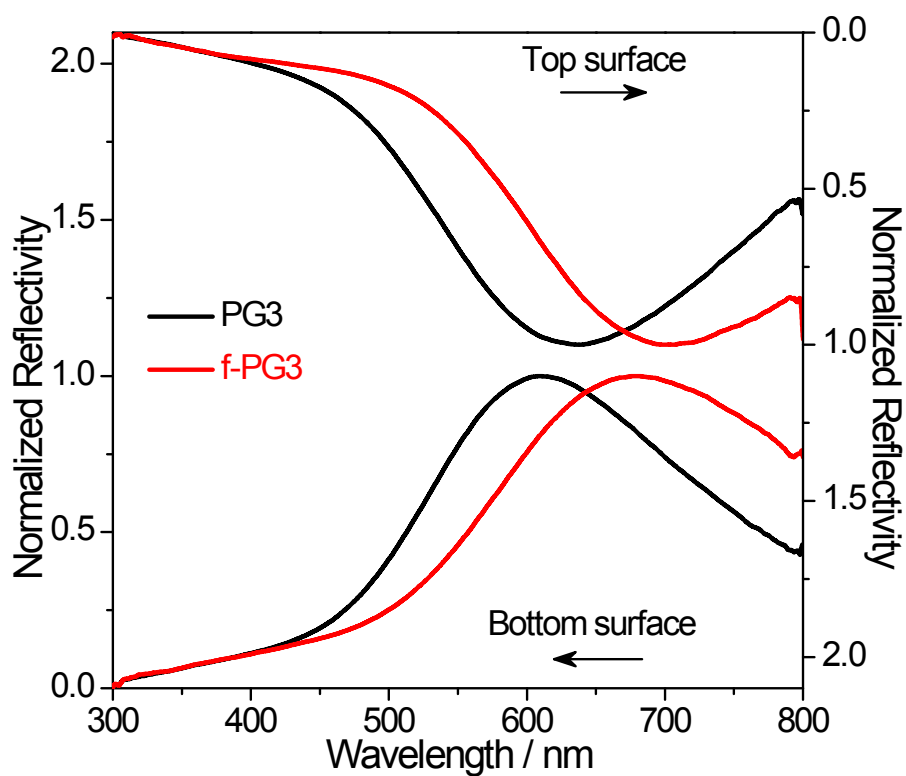


Fig. S14 Reflection spectra of PG3 and f-PG3 on both surfaces.

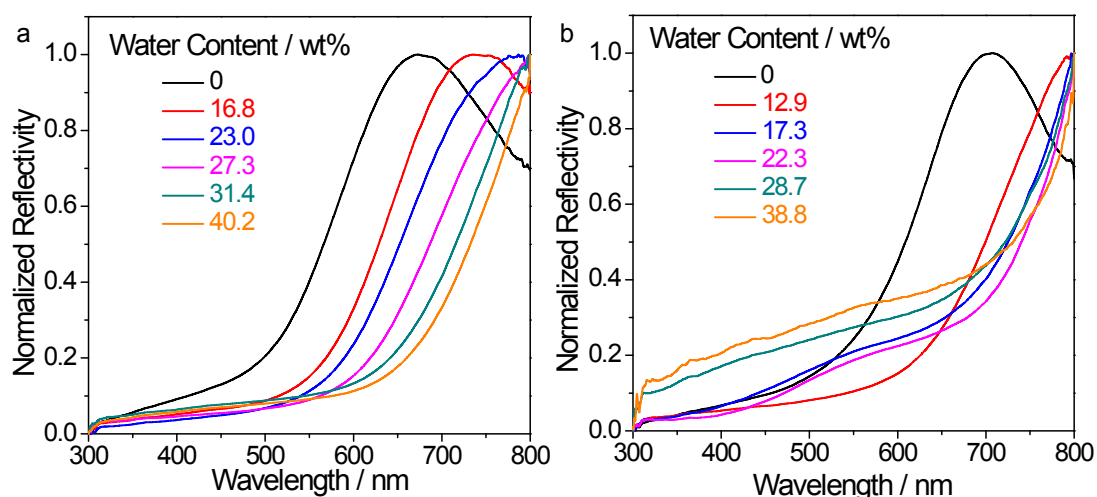


Fig. S15 Reflection spectra on the top surfaces of PG3 (a) and f-PG3 (b) as a function of the content of the absorbed water within the film.

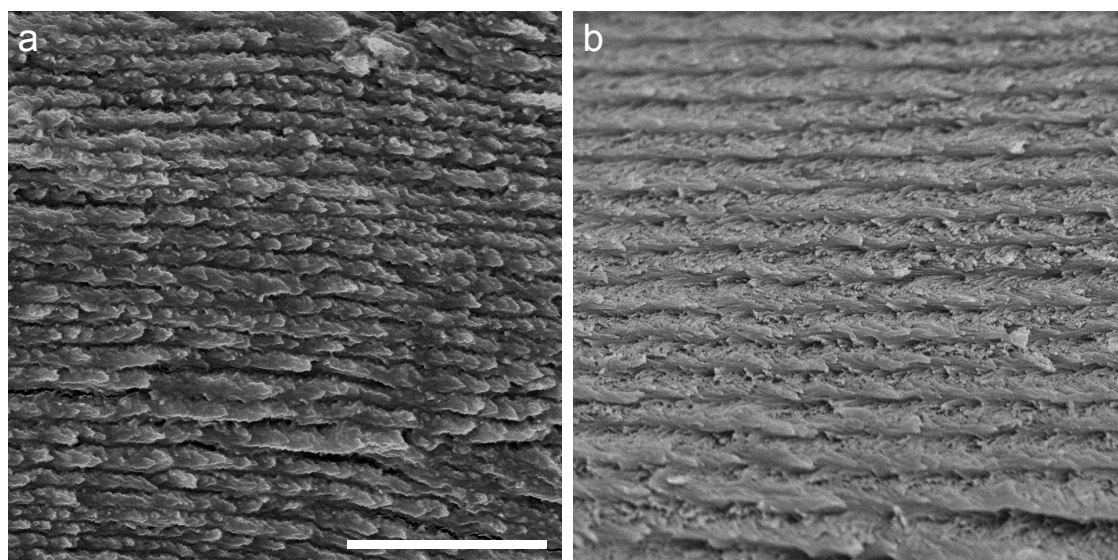


Fig. S16 SEM images of f-PG3 (a) and the film with the same composition but dried by SCCO_2 (b). The magnifications of the two images are the same with the scale bar to be 2.5 μm .

7. Additional results of the tests on the objects treated with different chemicals and those prepared from different films

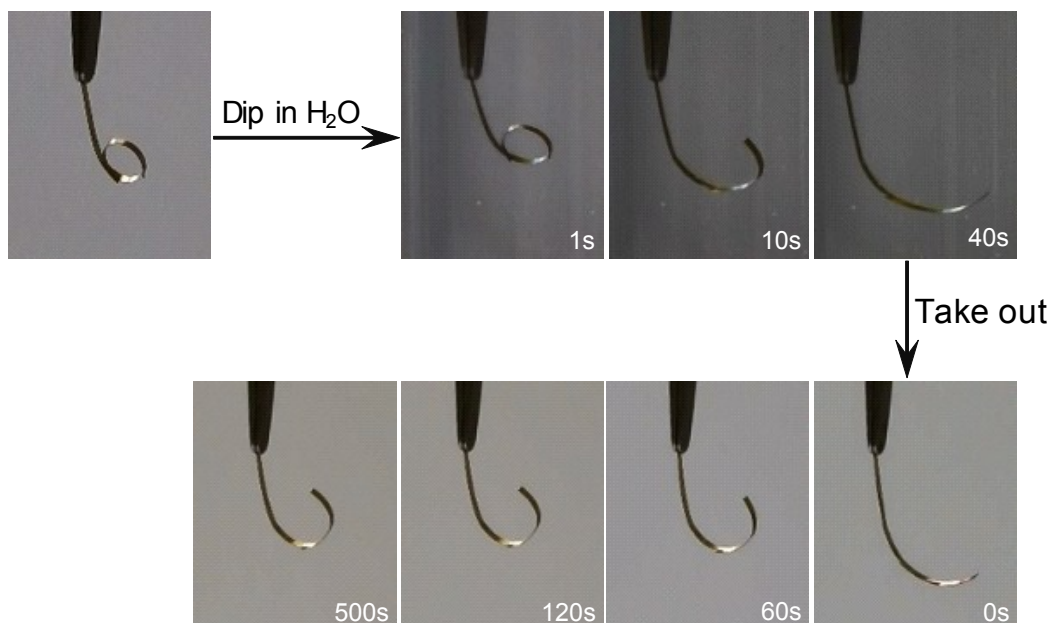


Fig. S17 Response of the film bar made from f-PG3 with a predefined shape of the Arabic numeral 6 toward wetting-drying circle.

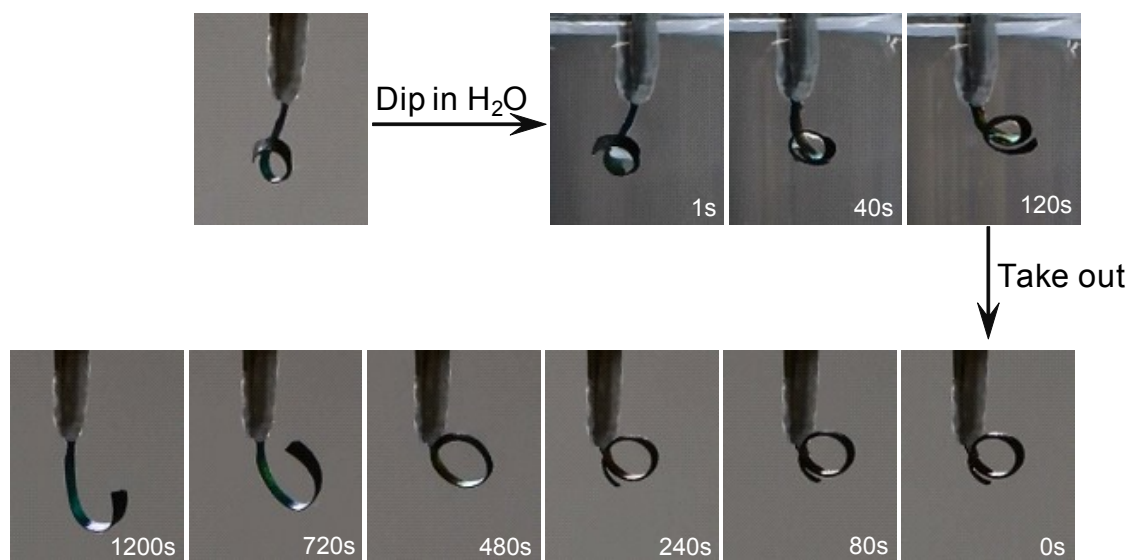


Fig. S18 Response of the latex/GO (LG) film bar with a predefined shape of the Arabic numeral 6 toward wetting-drying circle. The numeral was treated with FoA in the same way as that prepared by PG3. The thickness of the film bar is $\sim 160 \mu\text{m}$.

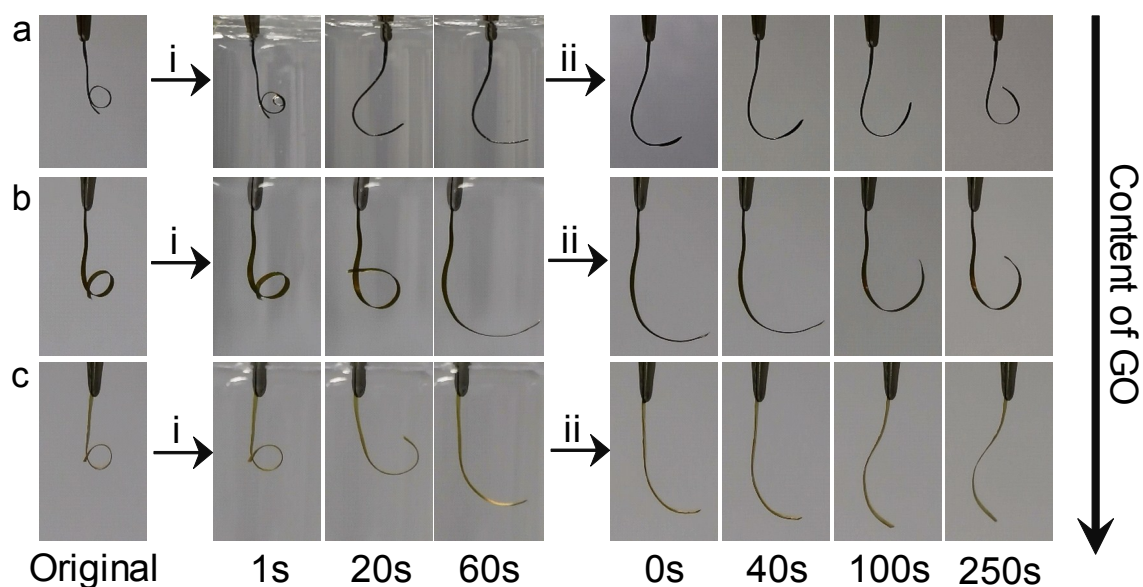


Fig. S19 Responses of the film bars with a predefined shape of the Arabic numeral 6 from PG2 (a), PG1 (b) and PG0 (c) toward wetting-drying circle. Each numeral was treated with FoA in the same way as that prepared by PG3. i) Dip in water; ii) Take out.

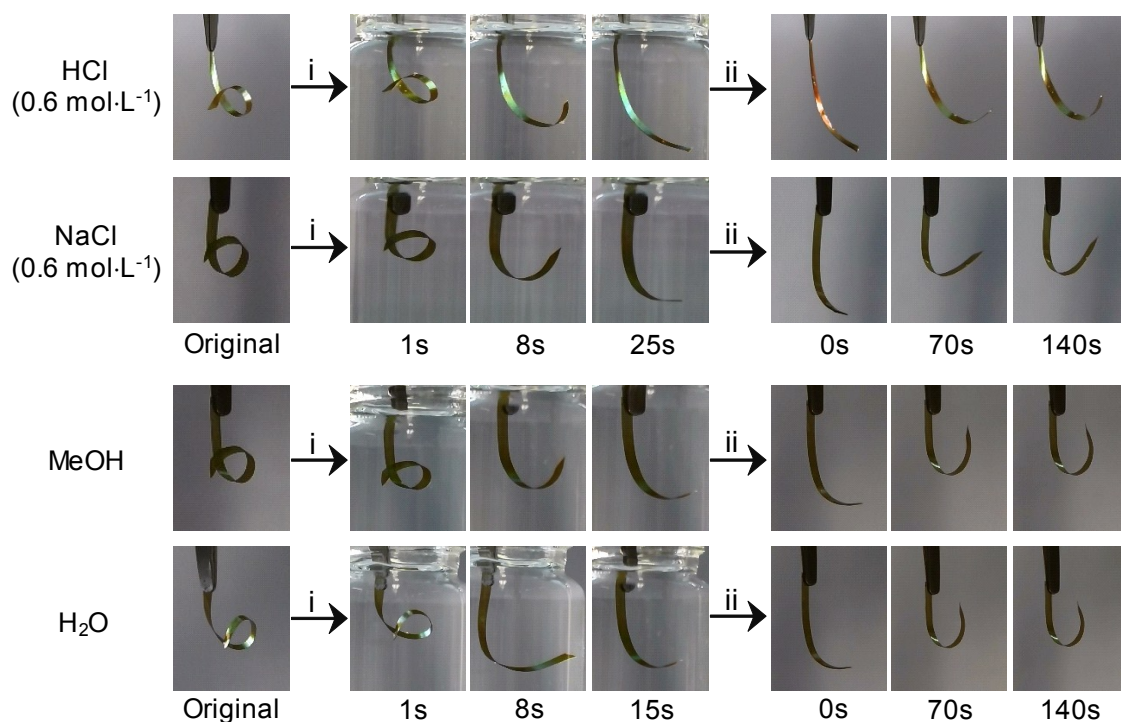


Fig. S20 Responses of the film bars with a predefined shape of the Arabic numeral 6 toward wetting-drying circle. The film bar was treated with various chemicals as illustrated. In all the cases, the thickness of the film bar is 53 μm .

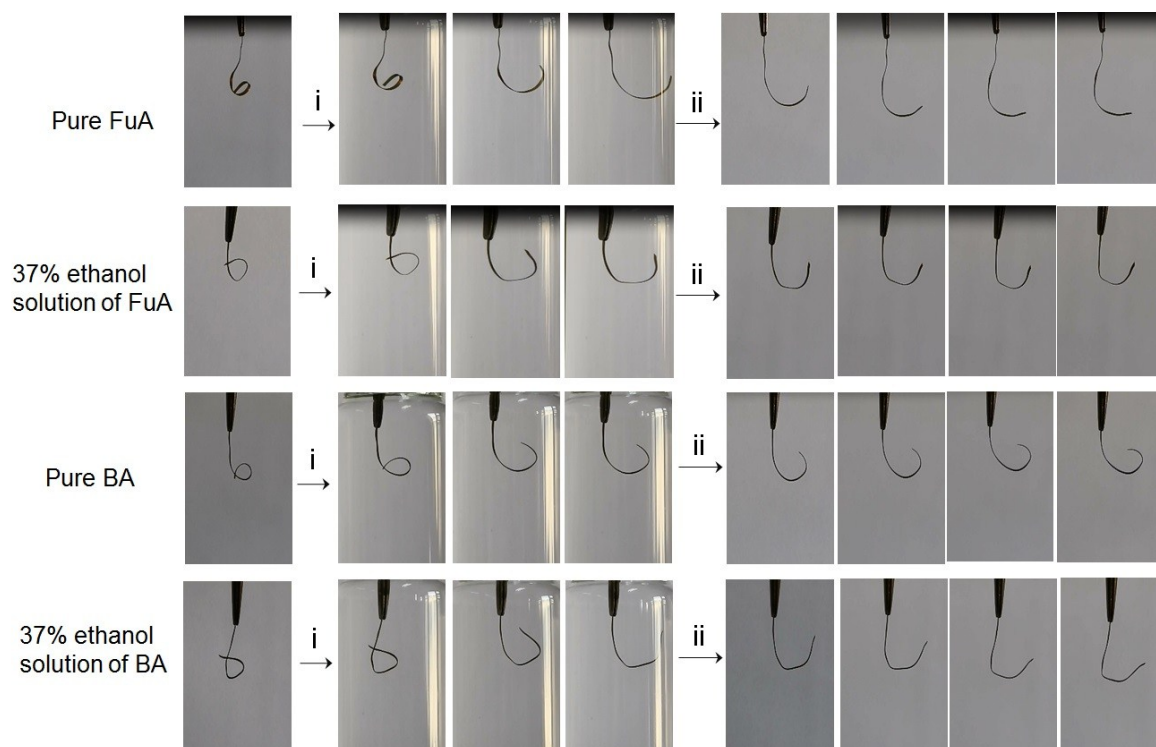


Fig. S21 Responses of the film bars with a predetermined shape of the Arabic numeral 6 toward wetting-drying circle. i) Dip in water; ii) Take out. The film bars were wetted in advance with absolute ethanol instead of water. Then they were treated with BA, FuA or their alcoholic solutions with a concentration of 37%.

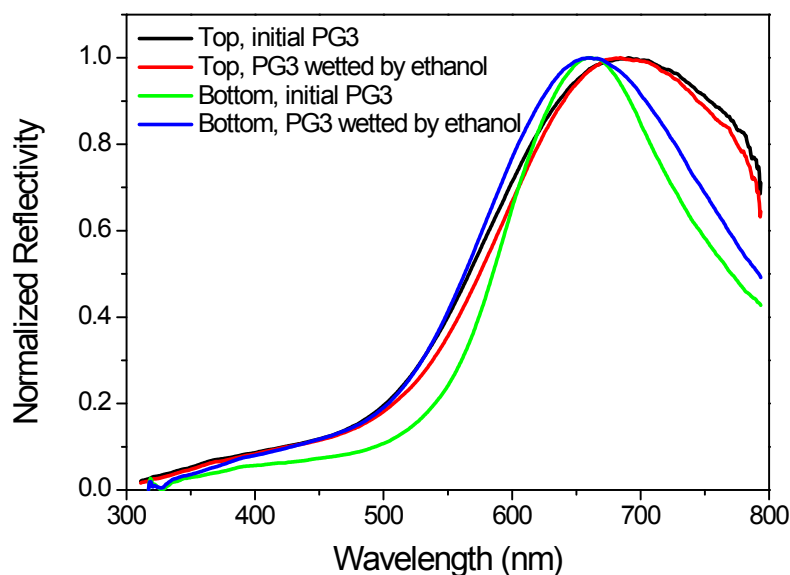


Fig. S22 Reflection spectra on top and bottom surfaces of PG3 before and after being wetted by ethanol for 5 h.

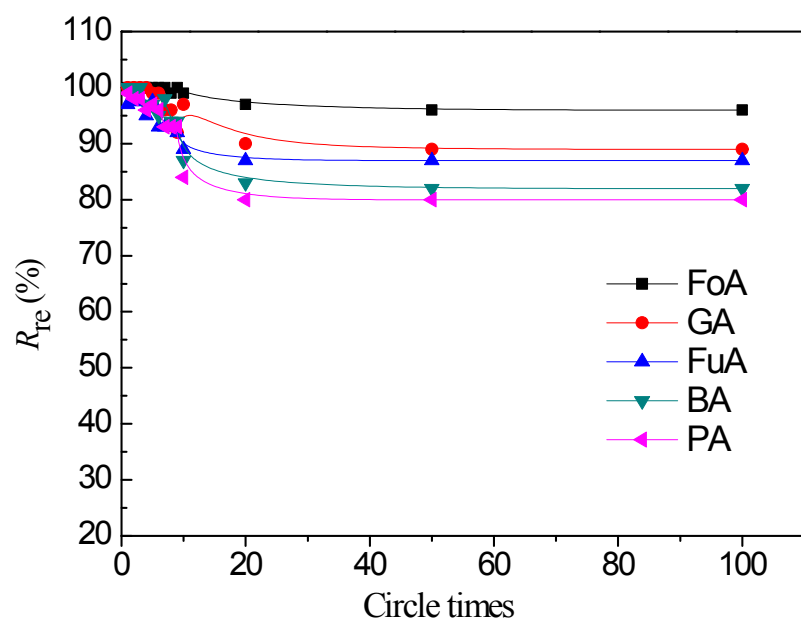


Fig. S23 Shape recovery rate (R_{re}) of the film bars treated by different aldehydes with a predetermined shape of the Arabic numeral 6 as a function of the wetting-drying circle time.